



Universiteit
Leiden
The Netherlands

Formation of Covalently Bonded Polycyclic Aromatic Hydrocarbons in the Interstellar Medium

Chen, T.

Citation

Chen, T. (2018). Formation of Covalently Bonded Polycyclic Aromatic Hydrocarbons in the Interstellar Medium. *Astrophysical Journal*, 866(2), 113. doi:10.3847/1538-4357/aae38f

Version: Not Applicable (or Unknown)

License: [Leiden University Non-exclusive license](#)

Downloaded from: <https://hdl.handle.net/1887/68724>

Note: To cite this publication please use the final published version (if applicable).



Formation of Covalently Bonded Polycyclic Aromatic Hydrocarbons in the Interstellar Medium

Tao Chen^{1,2} 

¹ Leiden University, Leiden Observatory, Niels Bohrweg 2, NL-2333 CA Leiden, Netherlands; chen@strw.leidenuniv.nl

² School of Engineering Sciences in Chemistry, Biotechnology and Health, Department of Theoretical Chemistry & Biology, Royal Institute of Technology, SE-10691, Stockholm, Sweden

Received 2018 August 23; revised 2018 September 20; accepted 2018 September 20; published 2018 October 19

Abstract

Photo-/ion-induced ionization and dissociation processes are commonly observed for polycyclic aromatic hydrocarbon (PAH) molecules. This work performs theoretical studies of PAHs and their fragments. Molecular dynamics simulations in combination with static quantum chemical calculations reveal that following a single hydrogen atom loss, the fragments, PAH-H, are extremely reactive. They catch a neighbor molecule within picoseconds to form a covalently bonded large molecule regardless of orientations/angles and temperatures. We calculate the infrared spectra of the covalently bonded molecules, which indicate that such species could be the carrier of unidentified infrared emission bands. It also implies that regular PAHs might be less abundant in space than what is expected.

Key words: astrochemistry – ISM: molecules – infrared: ISM – line: formation – methods: laboratory: molecular

1. Introduction

The broad IR emission bands at 3.3 μm , 6.2 μm , 7.7 μm , 8.6 μm , 11.2 μm , and 12.7 μm bands were discovered in 1973 (Leger & Puget 1984; Allamandola et al. 1989). They are commonly observed in a variety of astronomical objects, ranging from the Galaxy to extragalactic regions (Tielens 2008). Due to the absence of spectroscopic identification and lack of excitation mechanisms, for a long time, these bands were called unidentified infrared emission features (UIE; Leger & Puget 1984). Nowadays, these UIE bands are generally attributed to visible/UV photon-excited polycyclic aromatic hydrocarbon (PAH) molecules (Allamandola et al. 1989; Tielens 2008), in which the 3.3 μm band is attributed to the C–H stretching modes, the 6.2 and 7.7 μm bands to the C–C stretching modes, while 11.2 and 12.7 μm are attributed to the C–H out-of-plane bending modes of PAHs (Tielens 2008). With their compact and stable structure, PAHs are believed to be abundant and ubiquitous in the interstellar medium (ISM), locking up 10%–20% of the elemental carbon (Tielens 2008).

In the ISM, a number of different reactions related to PAHs can take place: following the absorption of UV photons from luminous stars, most of the time, PAHs will relax through IR vibrational relaxation (Allamandola et al. 1989; Tielens 2008), but there is the probability of photofragmentation and loss of H (C_2H_2 fragments have been indicated as dominant loss channels for small PAHs; Ekern et al. 1998; Jochims et al. 1999; West et al. 2012; Zhen et al. 2014), isomerization (Dyakov et al. 2006; Johansson et al. 2011; Solano & Mayer 2015; Simon et al. 2017; Trinquier et al. 2017), and ionization (Holm et al. 2011; Zhen et al. 2015). Large PAHs, on the other hand, may preferentially lose all of their H, and the resulting graphene sheet may isomerize to fullerenes such as C_{60} , which is very stable under interstellar conditions (Ekern et al. 1998; Berné & Tielens 2012; Zhen et al. 2014).

Fragmentation turns out to be crucial for molecular growth processes in PAH/fullerene clusters; e.g., recent works have shown that following the loss of C atoms, C_{119}^+ and C_{118}^+ could be formed in collisions between keV alpha particles and van

der Waals clusters of C_{60} fullerenes (Zettergren et al. 2013). In such experiments, a carbon atom or C_2 is knocked out directly from a C_{60} . The newly formed C_{59}^+ or C_{58}^+ radicals react with a neighbor C_{60} to form C_{119}^+ and C_{118}^+ within picoseconds (Seitz et al. 2013; Wang et al. 2014). A similar process has been observed in pyrene clusters following C and/or H losses (Delaunay et al. 2015) and in small hydrocarbon chain clusters (Gatchell et al. 2017) in which new molecules are formed following a direct knockout of atoms via Rutherford-like ion-atom scattering processes.

The formation of large PAHs following photodissociation processes in PAH clusters has been reported recently (Zhen et al. 2018b). However, those studies are multiple-step reactions, e.g., several H losses and barriers are required in the reactions (Zhen et al. 2018b), which can only be achieved through multiphoton processes (Montillaud et al. 2013; Andrews et al. 2016). Such formation processes might be less feasible in the ISM in comparison to single-photon processes, which are generally believed to be the carrier of UIE bands (Allamandola et al. 1985, 1989; Tielens 2008). In this work, we focus on exothermic and barrier-free reactions, which are accessible even in low-density and low-temperature astronomical environments. Due to the compact and stable structure, we choose the pyrene molecule for this study. Figure 1 shows three possible dissociation channels for H and H_2 losses from a pyrene ($\text{C}_{16}\text{H}_{10}$) molecule (Chen et al. 2015). The energy differences among these channels are rather small, e.g., for H losses, the lowest adiabatic dissociation energy is 5.09 eV (Ha in Figure 1), while the highest one is 5.33 eV (Hc in Figure 1; Chen et al. 2015). H_2 losses are competing processes against H loss from a PAH molecule; however, it involves several barriers, e.g., one or two barriers for hydrogen migrations and one barrier for H_2 dissociate from a PAH (Chen et al. 2015), in which the highest barriers are comparable with the dissociation energy of H losses (Chen et al. 2015). This article investigates several possible formation pathways, structures, and IR features of pyrene and pyrene-H/pyrene-2H. The dynamical formation processes and instant structures are studied using ab initio molecular dynamics simulations. The

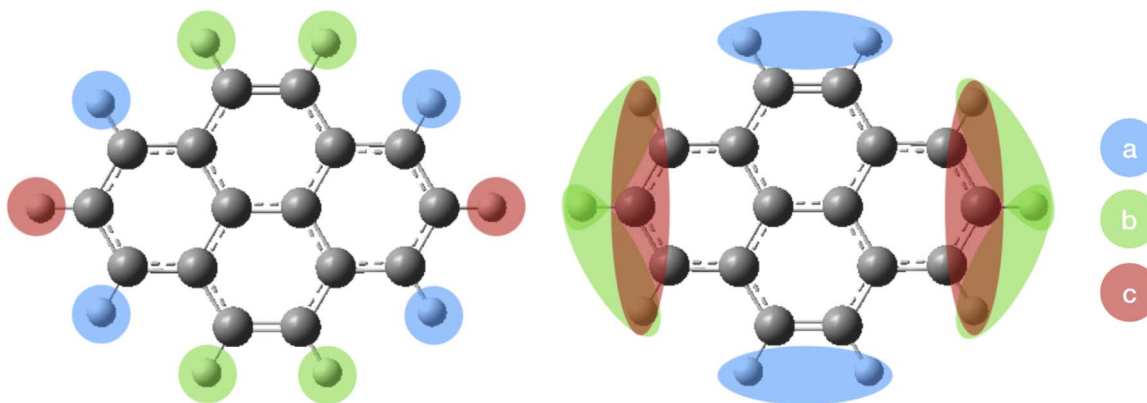


Figure 1. Three possible dissociation channels for the losses of H and H₂ from pyrene (C₁₆H₁₀). For H losses, hydrogens with the same color are identical in terms of dissociation energy. For H₂ losses, two hydrogens are linked using the same color; again, the H₂ with the same color are identical in energy.

Table 1
The Binding Energies and Geometries for the Benzene (C₆H₆) Dimer

Method	Binding energy (kcal/mol) ^a	Dimer distance (Å) ^b	C–C bond (Å) ^c	C–H bond (Å) ^c
B3LYP-D3/3-21G*	3.97	3.90	1.398	1.084
B3LYP-D3/6-311++G(2d,p)	2.96	3.95	1.392	1.084
Sinnokrot et al. (2002)	2.78	3.76
Tsuzuki et al. (2002)	2.48	3.94
Park & Lee (2006)	3.03	3.94	1.395	1.087

Notes.

^a The energies are measured for two parallel-displaced benzenes.

^b The distances are measured between the geometrical center of two parallel-displaced benzenes.

^c The bond lengths are measured for benzene monomers.

ground-state structures and IR features are calculated with static quantum chemical calculations.

2. Computational Details

Theoretical calculations are carried out using density functional theory (DFT) with the hybrid density functional B3LYP (Lee et al. 1988; Becke 1992) as implemented in the Gaussian 16 program (Frisch et al. 2016). All structures are optimized using the 6-311++G(2d,p) basis set. The vibrational frequencies are calculated for the optimized geometries to verify that these correspond to minima or first-order saddle points (transition states) on the potential energy surface (PES). We have taken the zero-point vibrational energy (ZPVE) into account. The ZPVE values are scaled by the empirical factor 0.965 to correct for anharmonic effects (Andersson & Uvdal 2005). In all cases, we have only considered the ground-state PES as the non-radiative decay for such a large molecule is very rapid: $\sim 10^{-12}$ s (Vierheilig et al. 1999; Zewail 2000). Only the lowest spin state is considered, which seems to be a well-justified approach to predict reasonable energies in comparison to the experimental results (Holm et al. 2011). The dispersion-corrected B3LYP-D3 (Grimme et al. 2011) is considered to account for the intermolecular forces in PAH clusters.

The dynamical processes are simulated using the Atom Centered Density Matrix Propagation (ADMP) molecular dynamics model (Iyengar et al. 2001; Schlegel et al. 2001, 2002). This method provides equivalent functionality to Born–Oppenheimer molecular dynamics at a considerably reduced computational cost (Schlegel et al. 2002). The functional of B3LYP in combination with the basis sets of 3-21G* is utilized

for the simulations. To take the weakly bonded systems into account, we consider the dispersion-corrected B3LYP-D3. To evaluate the accuracies of the functional and basis sets, the benzene dimer has been investigated. Table 1 shows the binding energies and geometries of the parallel-displaced benzene dimer. Moreover, the bond distances of the benzene monomer and the corresponding values from the literature (Sinnokrot et al. 2002; Tsuzuki et al. 2002; Park & Lee 2006) are also presented. One can see that B3LYP-D3/3-21G* produces a slightly higher value of the binding energy, but provides rather accurate geometries in comparison to other high-level calculations. This work focuses on the geometry changes in the dynamical system of PAH clusters; B3LYP-D3/3-21G* ought to be sufficient for such a study.

For the ADMP calculations, a step size of 0.3 fs was used for each system. The initial structure/positions of the molecules were optimized before running the molecular dynamics simulations. The initial velocity of each molecule was set to zero.

3. Results and Discussion

It has been shown that H and H₂ losses from PAHs are efficient fragmentation pathways for both ion-induced and photoinduced experiments (Dyakov et al. 2006; West et al. 2014; Chen et al. 2015).

To study the reactivity of pyrene-H_x ($x = 1$ or 2), we performed molecular dynamics simulations. The charged systems, i.e., pyrene + pyrene-H_x, which are positively charged, are investigated first. Figure 2 shows five snapshots from the molecular dynamics simulations. The initial geometry comprises an intact pyrene in combination with a pyrene-Ha

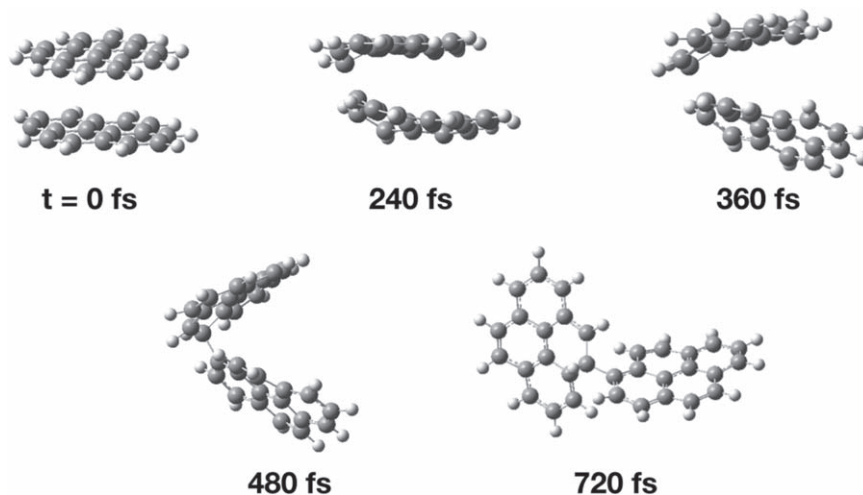


Figure 2. Five snapshots from molecular dynamics simulations showing the interaction between pyrene and pyrene-Ha (see Figure 1). A covalently bonded pyrene complex is formed without any external energy or initial velocity within a picosecond.

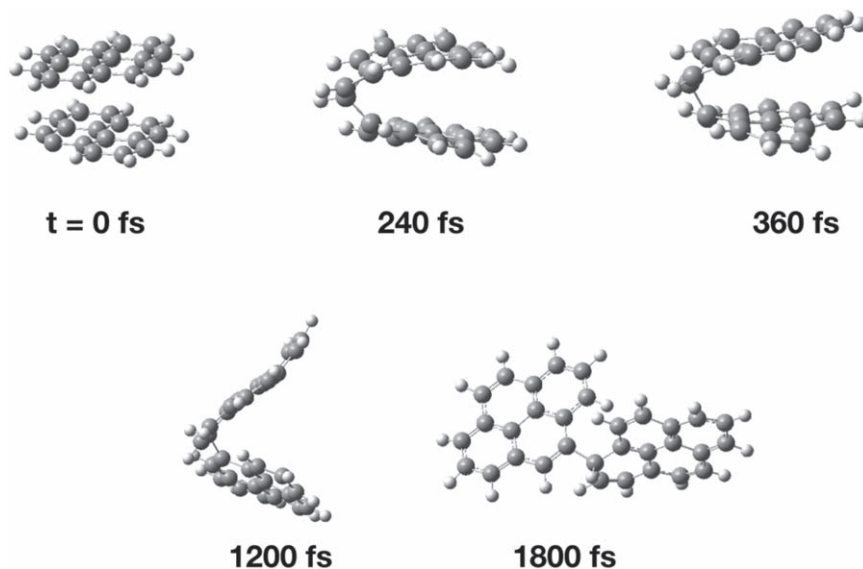


Figure 3. Five snapshots from molecular dynamics simulations showing the interaction between pyrene and pyrene-Hb (see Figure 1). A covalently bonded pyrene complex is formed without any external energy or initial velocity within a picosecond.

molecule (see Figure 1), which are oriented in a parallel position (stacked) and separated by ~ 3.5 Å (this value is the ground-state distance for van der Waals complexes found via time-independent DFT calculations at 0 K). It has been reported that for PAH clusters, the stacked structure corresponds to the most stable structure (Rapacioli et al. 2005).

The simulation shows that the molecules move close to each other rapidly in the beginning of the simulation, especially on the side where the hydrogen is lost, i.e., pyrene-Ha transform to a bent structure from a planar structure (see the second frame at 240 fs in Figure 2). Subsequently (the third frame at 360 fs in Figure 2), pyrene-Ha transforms back to a planar structure. However, an angled system is formed with an angle of $\sim 60^\circ$. The distance between the carbon atom (in pyrene-Ha) where Ha is located and the closest carbon atom in the intact pyrene remain almost unchanged (~ 1.65 Å). At 480 fs into the simulation, the angle between the molecules increases, and a covalent bond is formed between the molecules, with a bond length of ~ 1.55 Å. Finally, the molecules form a covalently bonded perpendicular system with a bond length of ~ 1.5 Å,

and they do not break or transform into other isomers until the end of the simulation (a few tens of picoseconds), i.e., the fifth frame in Figure 2 ought to be an equilibrated state/structure. We investigate different initial conditions, e.g., angle/orientation, distance, and temperature. It turns out that the formation of covalently bonded systems is very sensitive to the distance between molecules in comparison to the angle/orientation or temperature (see the discussion below for more details regarding the importance of the initial distance). If the initial geometry is set to a perpendicular orientation, or even at a low temperature (e.g., 4 K), the covalently bonded system will always be formed in the simulation. See the time-independent DFT calculations below for the reason for the independence of the initial orientation and temperature.

Similar reaction pathways have been observed for the pyrene and the pyrene-Hb molecule system (see Figure 1). However, the formation of the covalently bonded perpendicular system, i.e., the equilibrated state, is about twice slower than for the case of pyrene-Ha, and the formed structure is slightly different; see Figure 3 for details.

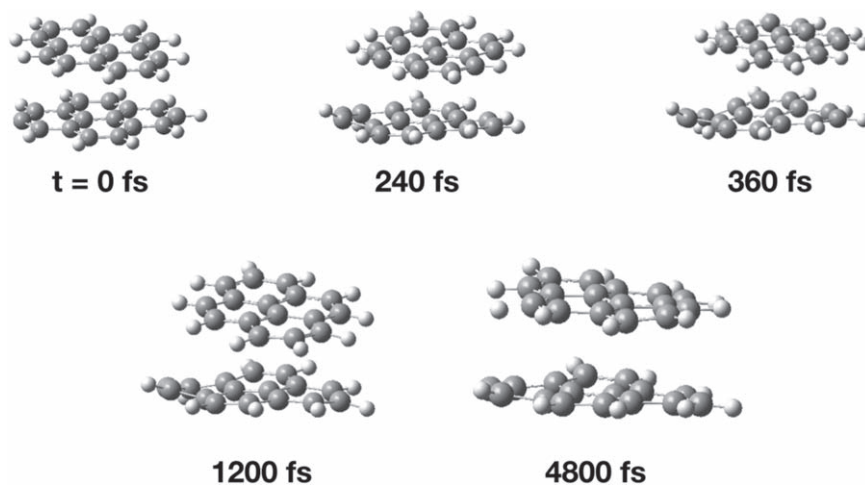


Figure 4. Five snapshots from molecular dynamics simulations showing the interaction between pyrene and pyrene-Hc (see Figure 1). No covalently bonded system is formed within 5 picoseconds.

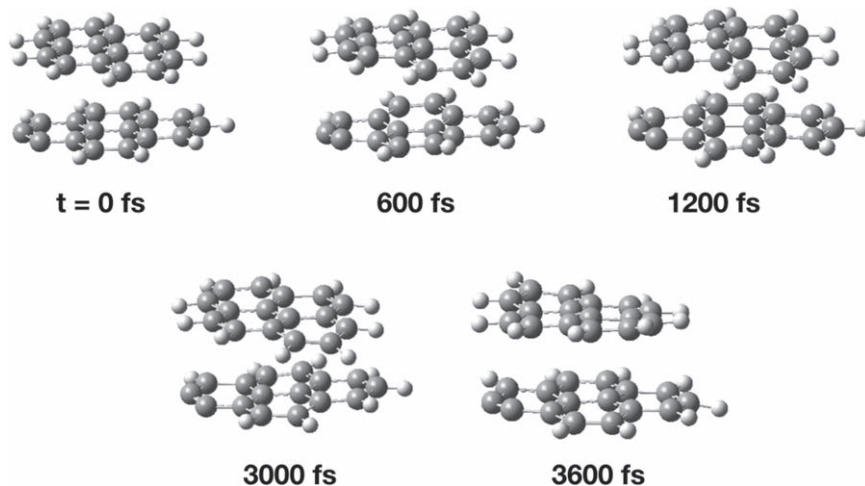


Figure 5. Five snapshots from molecular dynamics simulations showing the interaction between pyrene and pyrene-2Ha (see Figure 1). No covalently bonded system is formed within 4 picoseconds.

For the case of pyrene-Hc, no covalently bonded system is formed within the simulation time. Instead, a weakly bonded van der Waals dimer is formed with a separation of ~ 3.5 Å. See Figure 4 for details. We do not know why no covalently bonded molecule formed in such a case; it might be related to the fact that pyrene-Hc is a symmetric structure, which could reduce the reactivity of the radical.

We also study the neutral system, i.e., both molecules are neutral. However, for all possible single H-loss positions, none of the covalently bonded systems was formed; instead, weakly bonded van der Waals dimers are formed with a structure similar to that in Figure 4. In other words, the charge plays a vital role in the formation of covalently bonded large molecules.

The loss of molecular hydrogens (H_2) is a dominant dissociation channel in statistical fragmentation processes (Dyakov et al. 2006; West et al. 2014; Chen et al. 2015). As shown in our previous study, three H_2 loss pathways are the most energetically favorable (Chen et al. 2015); see Figure 1 for the positions. We study the reactivity of these three isomers for both neutral and charged systems. However, none of the covalently bonded systems was formed; only weakly bonded

van der Waals dimers are formed. See Figure 5 for an example of the structure (pyrene + pyrene-2Ha).

To clarify the essence of the reactions, we carried out static quantum chemical calculations. Figure 6 shows the calculated sequential H losses from pyrene in combination with pyrene-H. It turns out that the reaction between pyrene-H and pyrene is an exothermic reaction, i.e., there are attractive forces between these two species. It explains why the covalent bond is formed promptly as shown in the molecular dynamics simulations. In addition, we found that the dissociation energies of the hydrogens in between the molecules are rather low: 1.8–2.6 eV in comparison to ~ 5 eV for a regular PAH. These results indicate that the molecules tend to form a complex larger molecule at first, then lose all of the aliphatic hydrogens in between to form a planar PAH (Zhen et al. 2018b). It is important to note that transition states are involved for the formations and not shown in Figure 6. Therefore, large planar PAHs are even more difficult to form in reality in comparison to covalently bonded systems, as shown in Figure 6.

Figure 7 compares the calculated infrared spectra of a few molecules studied above and the observed IR spectrum of NGC 2023 and Orion Bar. The observational data are retrieved from the *Infrared Space Observatory* archive. The harmonic

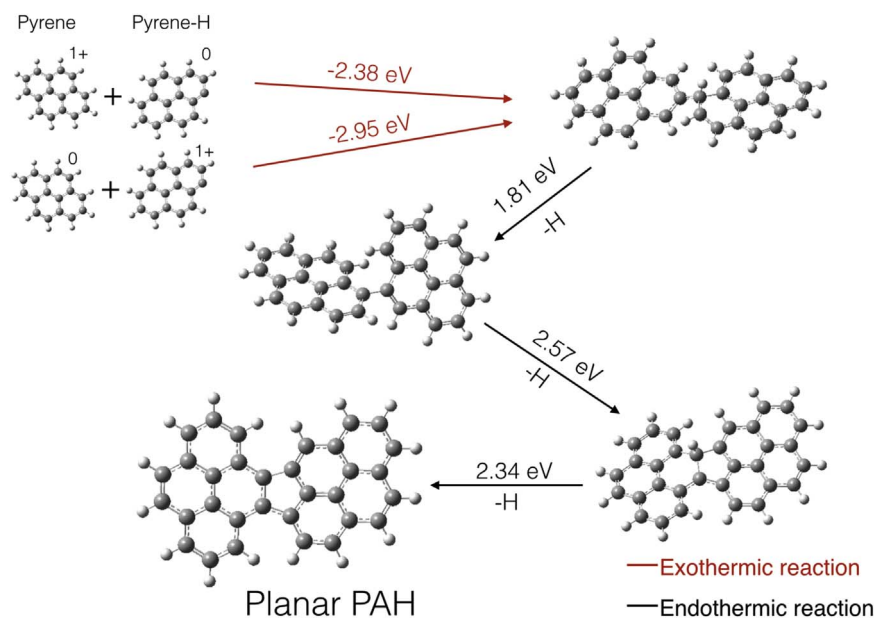


Figure 6. Calculated possible reaction pathways using B3LYP-D3/6-311++G(2d,p). The red arrows correspond to exothermic reactions, and the black arrows indicate endothermic reactions. The values on the arrows correspond to the dissociation energies of H losses or binding energies for the exothermic reactions.

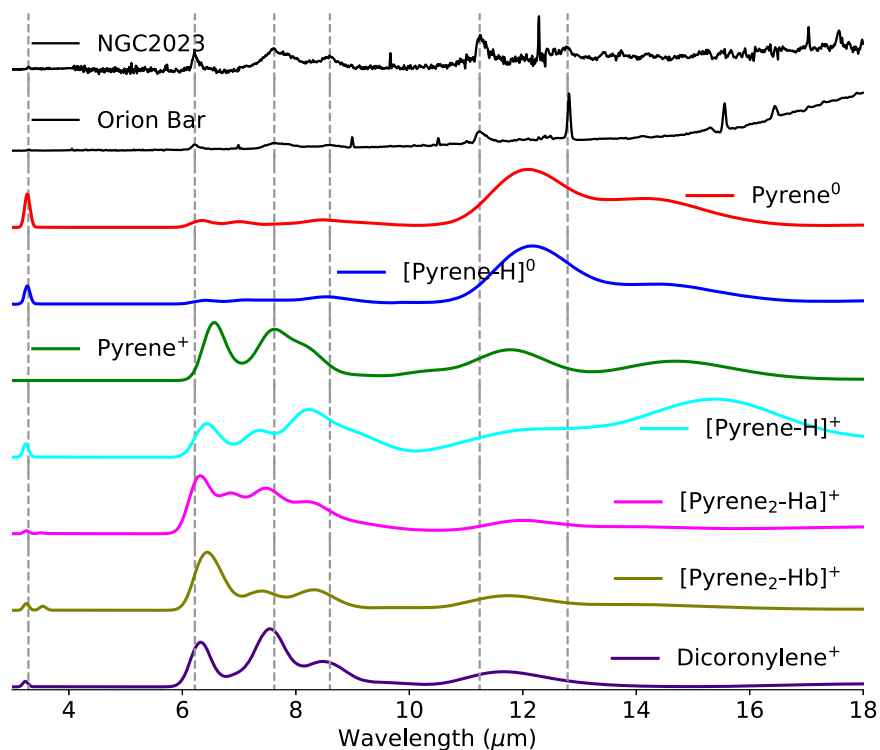


Figure 7. Observational IR spectrum of NGC 2023 and the Orion Bar, and calculated harmonic vibrational spectra of neutral and charged pyrene and pyrene-H, and covalently bonded pyrene, pyrene-H, and dicoronylene cation. The calculated spectra are scaled by 0.965 and broadened by 45 cm^{-1} to correct for anharmonic and temperature effects. The dashed lines represent some dominant bands that are commonly observed in the ISM (Tielens 2008).

vibrational spectra are calculated using B3LYP/6-311++G(2d,p). The calculated spectra are further scaled by 0.965 and broadened by 45 cm^{-1} to correct for anharmonic and temperature effects. Several prominent bands, e.g., the $3.3\text{ }\mu\text{m}$, $6.2\text{ }\mu\text{m}$, $7.7\text{ }\mu\text{m}$, $8.6\text{ }\mu\text{m}$, $11.2\text{ }\mu\text{m}$, and $12.7\text{ }\mu\text{m}$ bands, are marked with dashed lines. It is clear that the $3.3\text{ }\mu\text{m}$ band can be well explained by the C–H stretching of neutral PAHs, e.g., pyrene⁰ and [pyrene–H]⁰, as well as the covalently bonded system, i.e., [pyrene₂–Ha]⁺ and [pyrene₂–Hb]⁺. For

the pyrene cation, i.e., pyrene⁺, the $3.3\text{ }\mu\text{m}$ band is missing. The $6.2\text{ }\mu\text{m}$ band might be explained by the C–C stretching of charged PAHs. However, the covalently bonded system, especially [pyrene₂–Ha]⁺ agrees the best ($\leq 0.1\text{ }\mu\text{m}$) with the observations in terms of band positions. The $7.7\text{ }\mu\text{m}$ band matches pyrene⁺ and [pyrene₂–Ha]⁺ accurately in comparison to the other species as shown in Figure 7. The other bands cannot be explained by the molecules studied in this work; they might be attributed to larger covalently bonded systems, e.g., a

recent work shows that the bands 8.6 and 11.2 μm might be explained by the dicoronylene cation (Zhen et al. 2018a), which is also a covalently bonded system.

3.1. Conclusions

In this work, we performed a theoretical study of molecular dynamics simulations to investigate the reactivity of PAH radicals and PAH cations. The simulations show that PAH-H is very reactive and can form a covalent bond with a neighbor molecule on a timescale of picoseconds. For a pyrene molecule, all possible H-loss channels are tested—two (pyrene-Ha and pyrene-Hb) out of three isomers lead to the formation of a covalently bonded system, the last one, pyrene-Hc, leads to the formation of a weakly bonded van der Waals dimer. We tested the influence of the charge state for all possible H-loss channels. It turns out that the covalent bond between pyrene-Hx and pyrene can only be formed when one of them is a cation. Furthermore, we studied the H₂ losses from pyrene. Three possible H₂-loss channels for both neutral and charged systems are tested; however, no covalent bond was observed in the simulation. Instead, only weakly bonded van der Waals dimers are formed.

As mentioned in the introduction, in the ISM, PAH molecules are excited by the absorption of a photon. Several optional pathways might be undertaken to release the excess energy: (1) ionization, (2) IR emission, (3) isomerization, and (4) dissociation, e.g., H/H₂ losses. The molecules necessary for the reactions studied in this work, i.e., PAH-H and PAH⁺, can be efficiently formed following the absorption of single photons with energies below the Lyman limit. The MD simulations show that once these reactive species are produced, a covalently bonded system can be formed rapidly regardless of distance, orientation, and temperature.

For the large PAHs, ionization energies are low, i.e., the larger the PAH, the lower the ionization energies (Holm et al. 2011). Moreover, the dissociation energies for H loss from neutral PAHs are similar, independent of PAH size (Holm et al. 2011). Therefore, the formation of a covalent bond between PAH-H and PAH⁺ ought to be more frequent in comparison to small PAHs.

In addition, this study explains the odd–even pattern of hydrogen loss that is commonly observed in the mass spectra of PAHs for both ion-induced and photoinduced experiments (West et al. 2014; Chen et al. 2015). As the [PAH-H]⁺ radicals are so reactive, they catch a neighbor rapidly in the timescale of the experiments ($\sim\mu\text{s}$). Therefore, almost no single H-loss PAH reaches the detector. However, [PAH-2H]⁺ is relatively stable. Hence, a large amount of [PAH-2H]⁺ can be detected following the time-of-flight measurements (West et al. 2014; Chen et al. 2015).

This work is supported by the Swedish Research Council (contract No. 2015-06501). The facility is supported by the Swedish National Infrastructure for Computing (project No. SNIC 2018/5-8). The calculations were carried out on Kebnekaise and Abisko located at the High Performance Computing Center North (HPC2N).

ORCID iDs

Tao Chen  <https://orcid.org/0000-0003-4145-4300>

References

- Allamandola, L., Tielens, A., & Barker, J. 1985, *ApJ*, 290, L25
 Allamandola, L., Tielens, A., & Barker, J. 1989, *ApJS*, 71, 733
 Andersson, M. P., & Uvdal, P. 2005, *JPCA*, 109, 2937
 Andrews, H., Candian, A., & Tielens, A. 2016, *A&A*, 595, A23
 Becke, A. D. 1992, *JChPh*, 96, 2155
 Berné, O., & Tielens, A. G. 2012, *PNAS*, 109, 401
 Chen, T., Gatchell, M., Stockett, M. H., et al. 2015, *JChPh*, 142, 144305
 Delaunay, R., Gatchell, M., Rousseau, P., et al. 2015, *JPhCh*, 6, 1536
 Dyakov, Y. A., Ni, C.-K., Lin, S., Lee, Y., & Mebel, A. 2006, *PCCP*, 8, 1404
 Ekern, S. P., Marshall, A. G., Szczepanski, J., & Vala, M. 1998, *JPCA*, 102, 3498
 Frisch, M., Trucks, G., Schlegel, H., et al. 2016, Gaussian 16, v.B.01 (Wallingford, CT: Gaussian, Inc.)
 Gatchell, M., Delaunay, R., D'Angelo, G., et al. 2017, *PCCP*, 19, 19665
 Grimme, S., Ehrlich, S., & Goerigk, L. 2011, *JCoCh*, 32, 1456
 Holm, A. I., Johansson, H. A., Cederquist, H., & Zettergren, H. 2011, *JChPh*, 134, 044301
 Iyengar, S. S., Schlegel, H. B., Millam, J. M., et al. 2001, *JChPh*, 115, 10291
 Jochims, H., Baumgärtel, H., & Leach, S. 1999, *ApJ*, 512, 500
 Johansson, H. A., Zettergren, H., Holm, A. I., et al. 2011, *JChPh*, 135, 084304
 Lee, C., Yang, W., & Parr, R. G. 1988, *PhRvB*, 37, 785
 Leger, A., & Puget, J. 1984, *A&A*, 137, L5
 Montillaud, J., Joblin, C., & Toubanc, D. 2013, *A&A*, 552, A15
 Park, Y. C., & Lee, J. S. 2006, *JPCA*, 110, 5091
 Rapacioli, M., Calvo, F., Spiegelman, F., Joblin, C., & Wales, D. 2005, *JPCA*, 109, 2487
 Schlegel, H. B., Iyengar, S. S., Li, X., et al. 2002, *JChPh*, 117, 8694
 Schlegel, H. B., Millam, J. M., Iyengar, S. S., et al. 2001, *JChPh*, 114, 9758
 Seitz, F., Zettergren, H., Rousseau, P., et al. 2013, *JChPh*, 139, 034309
 Simon, A., Rapacioli, M., Rouaut, G., Trinquier, G., & Gadéa, F. 2017, *RSPTA*, 375, 20160195
 Sinnokrot, M. O., Valeev, E. F., & Sherrill, C. D. 2002, *JChS*, 124, 10887
 Solano, E. A., & Mayer, P. M. 2015, *JChPh*, 143, 104305
 Tielens, A. G. G. M. 2008, *ARA&A*, 46, 289
 Trinquier, G., Simon, A., Rapacioli, M., & Gadéa, F. X. 2017, *MolAs*, 7, 37
 Tsuzuki, S., Honda, K., Uchimaru, T., Mikami, M., & Tanabe, K. 2002, *JChS*, 124, 104
 Vierheilig, A., Chen, T., Waltner, P., et al. 1999, *CPL*, 312, 349
 Wang, Y., Zettergren, H., Rousseau, P., et al. 2014, *PhRvA*, 89, 062708
 West, B., Joblin, C., Blanchet, V., et al. 2012, *JPCA*, 116, 10999
 West, B., Useli-Bacchitta, F., Sabbah, H., et al. 2014, *JPCA*, 118, 7824
 Zettergren, H., Rousseau, P., Wang, Y., et al. 2013, *PhRvL*, 110, 185501
 Zewail, A. H. 2000, *JPCA*, 104, 5660
 Zhen, J., Candian, A., Castellanos, P., et al. 2018a, *ApJ*, 854, 27
 Zhen, J., Castellanos, P., Paardekooper, D. M., et al. 2015, *ApJL*, 804, L7
 Zhen, J., Castellanos, P., Paardekooper, D. M., Linnartz, H., & Tielens, A. G. 2014, *ApJL*, 797, L30
 Zhen, J., Chen, T., & Tielens, A. G. 2018b, *ApJ*, 863, 128